The Astrophysical Journal, 654:338–346, 2007 January 1

SPITZER OBSERVATIONS OF THE GIANT MOLECULAR CLOUD W3

Gerald T. Ruch, Terry J. Jones, Charles E. Woodward, Elisha F. Polomski, and Robert D. Gehrz
Department of Astronomy, University of Minnesota, Minneapolis, MN; gruch@astro.umn.edu

and

S. T. Megeath
Havard-Smithsonian Center for Astrophysics, Cambridge, MA; and
Ritter Observatory, Department of Physics and Astronomy, University of Toledo, Toledo, OH
Received 2006 May 4; accepted 2006 August 31

ABSTRACT

We present new images of the giant molecular cloud W3 obtained with the Infrared Array Camera (IRAC) and the Multiband Imaging Photometer for *Spitzer* (MIPS) on board the *Spitzer Space Telescope*. The images encompass the star forming regions W3 Main, W3(OH), and a region that we refer to as the Central Cluster, which encloses the emission nebula IC 1795. We present a star count analysis of the point sources detected in W3. The star count analysis shows that the stellar population of the Central Cluster, when compared to that in the background, contains an over density of sources. The Central Cluster also contains an excess of sources with colors consistent with Class II young stellar objects (YSOs). An analysis of the color-color diagrams also reveals a large number of Class II YSOs in the Central Cluster. Our results suggest that an earlier epoch of star formation created the Central Cluster, created a cavity, and triggered the active star formation in the W3 Main and W3(OH) regions. We also detect a new outflow and its candidate exciting star.

Subject headings: infrared: ISM — infrared: stars — ISM: individual (W3) — stars: formation — stars: pre–main-sequence — stars: statistics —

Online material: machine-readable table

1. INTRODUCTION

Infrared imaging, with its ability to probe deeply into clouds of gas and dust where stars are known to form, has proven to be an essential tool in the study of star-forming regions. The instruments on board the *Spitzer Space Telescope* are providing new insights into the star formation process in numerous Galactic and extragalactic regions. The sensitive detectors of the Infrared Array Camera (IRAC; Fazio et al. 2004) and the Multiband Imaging Photometer for *Spitzer* (MIPS; Rieke et al. 2004) allow us to probe more deeply into nearby regions as well as obtain detailed views of more distant regions. As part of our Guaranteed Time Observation (GTO) program designed to investigate the star formation process (PID 124, PID 127) we have obtained IRAC and MIPS images of the W3 star-forming region with the intent of obtaining a complete census of the young stellar population.

The W3 complex is a region of ongoing star formation located at a distance of 1.95 kpc (Xu et al. 2006) toward the Perseus spiral arm. It is part of a larger complex including W4 that lies in the Galactic plane at the edge of the Perseus chimney, a Galactic superbubble extending 230 pc above the Galactic plane (Oey et al. 2005). Oey et al. (2005) argue that the W3/W4 complex is an example of hierarchical triggered star formation at the edge of a superbubble. An analysis at optical wavelengths of the stellar population of IC 1795, a component of W3, is presented by Oey et al. (2005) showing that this region may be the intermediate stage of three generation triggered star formation.

W3 itself is subdivided into three main knots of molecular gas known as W3 Main, W3 North, and W3 OH. The area known as W3 Main contains several compact and ultracompact H II regions (Wynn-Williams 1971; Harris & Wynn-Williams 1976) and several luminous infrared sources (Wynn-Williams et al. 1972) driven by a collection of embedded O and B stars (Ojha et al. 2004; Megeath et al. 1996). Megeath et al. (1996) demonstrate through near-infrared observations that the W3 Main core also contains a young cluster of low-mass ($\lesssim 2\ M_{\odot}$) YSOs. The W3(OH) region is a well-known star formation region that contains an ultracompact H II region and a hot molecular core (Turner & Welch 1984), several OH and methanol masers, and a deeply embedded young O7–O9 star (Dreher & Welch 1981).

YSOs were originally classified according to the spectral index defined by Adams et al. (1987). Sources with rising spectral energy distributions (SEDs) in the 1–25 μm region were labeled Class I, those with SEDs peaking in the near-IR and falling at longer wavelengths were labeled Class II, and those with rapidly falling SEDs, approaching Rayleigh-Jeans behavior, were labeled Class III. This classification scheme was interpreted as an evolutionary sequence, with Class I being the youngest and Class III being the most evolved. Class I sources are embedded protostars surrounded by an in-falling envelope of gas and dust. Class II sources are stars surrounded by a disk of gas and dust within which planetesimal formation is presumed to be taking place. Class III sources are evolved systems where the majority of the gas and dust has dissipated and planetary formation has ceased.

New IRAC and MIPS observations of the W3 region including W3 Main and W3(OH) are presented here. A three color image of the observed region is presented in Figure 1. In § 3.1 and § 3.2 we use star count analysis and interpretation of color-color diagrams to characterize the stellar population in W3. In § 3.1 we show that the region that we refer to as the Central Cluster, which encloses a known cluster around the emission nebula IC 1795, contains a cluster of sources with intrinsic IR excess whose colors are consistent with Class II YSOs. Reddening due to extinction is ruled out as a possible explanation for the excess of red sources. In § 3.2 we explore the location, both spatially and on the color-color diagram, of the subset of sources that are detectable

FIG. 1.—Three-color IRAC image of W3 (logarithmic flux stretch). 3.6 μm is coded blue, 4.5 μm is coded green, and 8.0 μm is coded red.

in all four IRAC bands. We find that a large fraction of these sources are Class II YSOs. In addition, we find that over half of the sources identified as Class II YSOs are located in the Central Cluster. At the edge of the cluster, we detect a previously unknown bipolar outflow along with its source.

We conclude that W3 may provide an example of triggered star formation, an hypothesis suggested by Oey et al. (2005). In addition to having a concentration of YSOs, the Central Cluster is relatively free of molecular gas as traced by CO (Kramer et al. 2004). The lack of highly luminous young objects along with low CO column densities leads us to surmise that the Central Cluster resides in a cavity with the highly luminous regions W3 Main and W3(OH) and the new outflow on its boundary. We suggest that the Central Cluster is the result of an earlier episode of star formation that created a cavity in the molecular gas and that W3 Main, W3(OH), and the new outflow source are the results of triggered star formation at the edge of this cavity.

2. OBSERVATIONS AND DATA REDUCTION

W3 was observed with IRAC on 2004 January 10 UT under our GTO program, PID 127. Data was obtained in mapping mode for a $25\farcm4 \times 27\farcm6$ field centered at J2000 R.A. $2^{h}26^{m}34\fs4$ and decl. $61^{\circ}58'33\farcs8$ in all four IRAC bands. We identify the four IRAC bands by their central wavelengths; band 1 at 3.6 μm, band 2 at 4.5 μm, band 3 at 5.8 μm, and band 4 at 8.0 μm. All IRAC images were taken in high-dynamic range (HDR) mode with three exposures at each dither position, two at 10.4 s and one at 0.4 s. Three dithers per pointing were taken using the small cycling dither pattern for a total integration time of 63.6 s per pixel once the frames were combined. The raw data was processed with IRAC pipeline version S11.0.2. The post-BCD module `hdr_mask.pl` provided by the *Spitzer* Science Center was applied to replace saturated pixels in the long exposure frames with those from the short exposure frames. The final mosaics were created using the 2005 May 9 version of MOPEX (Makovoz & Khan 2005). A three-color image created using the final mosaics is presented in Figure 1. The luminous infrared sources IRS 4 and IRS 5 in W3 Main as well as the ultracompact H II region and hot molecular core of W3(OH) remain saturated in our final mosaics.

The MIPS observations were carried out on 2004 February 4 UT under GTO program PID 127. Images were taken in scan map mode using the fast scan speed for an average exposure time of 36 s per pixel once the frames were combined. The raw data were processed and the final mosaics created with pipeline version S10.0.3. The areas around W3 Main and W3(OH) are badly saturated in all MIPS bands, but some useful data was obtained away from these areas at 24 μm. We use only the 24 μm band for our analysis of the stellar population.

TABLE 1
SOURCE COUNTS

Bands (μm)	No. of Sources
3.6 and 4.5	7196
5.8 and 8.0	329
3.6, 4.5, 5.8, and 8.0	295
3.6, 4.5, 5.8, 8.0, and 24.0	38

Point-source extraction on the final mosaics was conducted using a version of DAOPHOT (Stetson 1987) modified by the Galactic Legacy Infrared Mid-Plane Survey Extraordinaire (GLIMPSE) team to perform photometry in environments with highly variable backgrounds[1]. Point-source detection in a region as complex as W3 is complicated by spurious detections of sources that are actually knots of diffuse emission. Over 7000 point sources were detected at 3.6 and 4.5 μm, making visual verification of each detection unwieldy. Instead, we carried out point-spread function (PSF) fitting for each detection and used the resulting signal-to-noise ratio, which is based in part on the goodness of fit to the PSF, to reject the nonstellar detections. We find that a signal-to-noise ratio cutoff of 5 at 3.6 and 4.5 μm and 8 at 5.8 and 8.0 μm eliminates the majority of spurious detections while rejecting only a small fraction of actual point sources. We also discuss only those sources with detections that correlate in at least two IRAC bands. The number of correlated source counts is tabulated in Table 1. Careful measurement of the residual images for isolated sources away from areas of high-background variability shows that the uncertainty, at least in the isolated regions, is $\leq$10%. Final magnitudes were calculated using the following zero points; 280.9 ± 4.1 Jy at 3.6 μm, 179.7 ± 2.6 Jy at 4.5 μm, 115.0 ± 1.7 Jy at 5.8 μm, 64.1 ± 0.9 Jy at 8.0 μm[2], and 7.14 ± 0.815 Jy at 20.4 μm[3].

3. RESULTS

Figure 2 is a 3.6 μm image of W3 with several important and well known regions labeled. The large bright area in the northwest is the well-studied region known as W3 Main. In the southeast is another well-studied region known as W3(OH). Between these two bright regions is an area that we have defined as the Central Cluster. Our Central Cluster encloses the emission nebula IC 1795, marked by an asterisk in Figure 2, and overlaps the region around IC 1795 studied by Oey et al. (2005). We have also chosen two areas, one to the east and one to the southwest, labeled as background that are relatively free of diffuse emission for use as comparison fields.

Figure 3 is a $5\farcm3 \times 6\farcm1$ 8.0 μm contour map of the W3 main region with contours spaced every 0.2 dex from 2.6 (4.0×10^2 MJy sr^{-1}) to 3.8 (1.6×10^4 MJy sr^{-1}). The map covers the

[1] For more details concerning the photometry routine, see the GLIMPSE document at http://www.astro.wisc.edu/glimpse/photometry_v1.0.pdf and associated documents at http://www.astro.wisc.edu/glimpse/docs.html.

[2] Infrared Array Camera Data Handbook, version 2.0, at http://ssc.spitzer.caltech.edu/irac/dh/iracdatahandbook2.0.pdf.

[3] Multiband Imaging Photometer for *Spitzer* (MIPS) Data Handbook, version 3.2.1, at http://ssc.spitzer.caltech.edu/mips/dh/mipsdatahandbook3.2.pdf.

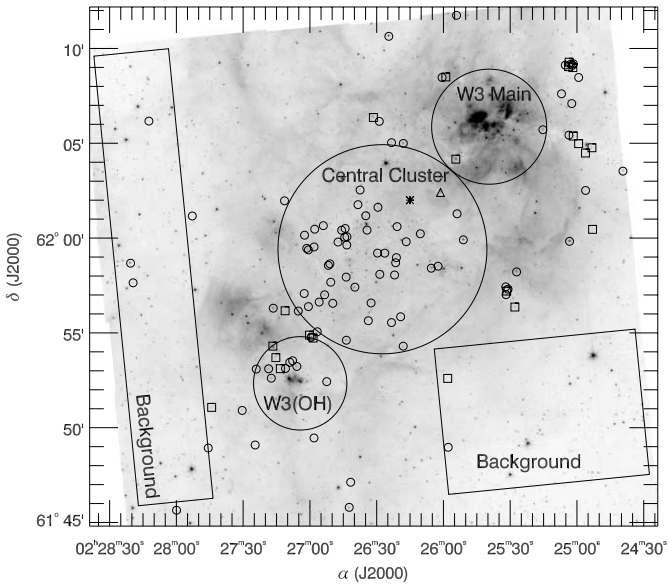

FIG. 2.—3.6 μm image of the W3 mosaic with regions of interest marked. W3 Main is in the northwest, W3(OH) is in the southeast, and the region we have defined as the Central Cluster is between the two. The Central Cluster encloses the emission nebula IC 1795 whose position is marked by an asterisk. The circles represent Class II YSOs and the squares represent Class I YSOs (see Fig. 7). We find a concentration of Class II objects in the Central Cluster region. Marked by a triangle near the northwest edge of the Central Cluster is the location of the outflow source discussed in § 3.3.

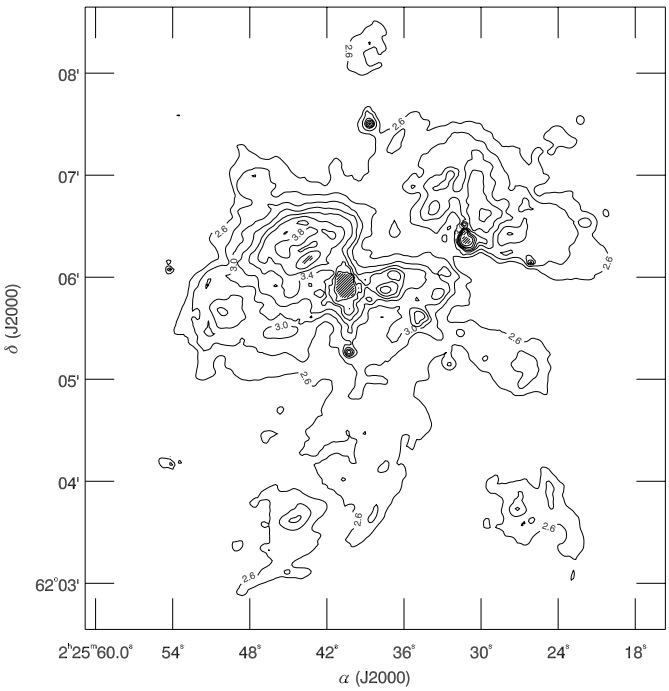

FIG. 3.—8.0 μm contour map of the W3 Main region. Contours represent log (MJy sr^{-1}) and are spaced 0.2 dex apart from 2.6 to 3.8. Areas with hash marks are inside the 4.0 isophot and are saturated.

well known bright infrared sources IRS 4 and IRS 5 (Wynn-Williams et al. 1972) as well as several compact and ultracompact H II regions. IRS 4 and IRS 5, as well as the ultracompact H II region and hot molecular core in W3(OH) are saturated in all four IRAC bands so we are unable to present IRAC fluxes for these sources. In Table 2 we present IRAC fluxes of the detectable embedded point sources associated with the compact H II regions W3A, W3H, W3J, and W3K. Fluxes for these sources were measured using the same PSF fitting routines in DAOPHOT that were used for all of the photometry presented here. The SEDs of these sources, that were rising in the near-IR bands (Ojha et al. 2004), continue to rise through all four IRAC bands. We assume that emission from circumstellar material is being detected. Figure 4 is a gray scale 8.0 μm image showing the locations of sources in Table 2 and several known compact and ultracompact H II regions.

3.1. *Star Counts*

Insight into the nature of the stellar population of W3 can be gained through star count analysis. In this section, the population of sources in the Central Cluster is compared to that in the background by examining star counts versus $[3.6] - [4.5]$ and $[5.8] - [8.0]$ colors. An overdensity of sources is detected in the Central Cluster. In addition, we find a large population of sources with colors consistent with Class II YSOs within the Central Cluster.

Before performing star count analysis, it is important to understand the completeness of our sample. We have obtained a completeness estimate by comparing the source counts in our background region to a model of the expected Galactic contamination (Garwood & Jones 1987). The results of this comparison are presented in the top plot of Figure 5. The plots in Figure 5 show counts per square arcminute versus K-band magnitude in both the background region and in the Central Cluster. The histograms represent our data and the diamonds represent the model predictions. We translated our 3.6 μm magnitudes into approximate K-band magnitudes as follows. We first found all sources in our background patch that had a corresponding identification in the Two Micron All Sky Survey (2MASS) catalog. Using these stars, a mean $K-[3.6]$ value of 0.32 ($\sigma = 0.2$) was determined. This mean $K-[3.6]$ value was then added to each object in our sample and an approximate the K-band luminosity function was created. Assuming that our background region contains primarily Galactic field stars, the top panel in Figure 5 represents an estimate of our completeness. The actual counts remain reasonably close to the model predictions up to $K \sim 15$. Beyond $K \sim 15$ there is a sharp dropoff. The bottom panel of Figure 5 shows a clear excess of sources at magnitudes less than $K \sim 15$ in the Central Cluster. Given that our completeness drops off rapidly at magnitudes greater than 15 and we see an excess of sources in the Central Cluster at magnitudes less than 15, the following discussion of star counts is limited to sources with $[3.6] \leq 15$.

We now use source counts as a function of color to compare the stellar population of the Central Cluster to that of the background. Figure 6 shows counts per square arcminute versus $[3.6] - [4.5]$ color in the top row and counts per square arcminute versus $[5.8] - [8.0]$ color in the bottom row. The bin size is 0.15 mag in the top row, on the order of the error in the color. The bin size in the bottom row was increased to 0.2 mag due to low source counts in the long wavelength bands. The left column shows counts in the Central Cluster, the middle column shows counts in the background regions, and the right column shows the difference. The error bars are based on the square root of the number of counts in each bin.

The upper panels of Figure 6 reveal both an overall excess of sources and an excess of red sources in the Central Cluster with respect to the background. Summing the difference curve we see an over density of sources in the Central Cluster of 4.3 ± 0.4 sources arcmin^{-2}. The red excess seen in the difference curve could be due to reddening, a population of sources with infrared excess, or a combination of the two. However, reddening can be ruled out as the major contributor. Using the tabulated extinction values from Indebetouw et al. (2005) and assuming a conservative value of A_V/A_K of 7.5, we find that a $[3.6] - [4.5]$ color of

TABLE 2
IRAC Fluxes of Embedded Sources in W3 Main

Name[a]	R.A.	Decl.	Flux (mJy)			
			3.6 μm	4.5 μm	5.8 μm	8.0 μm
IRS 2 (W3A)	02 25 44.37	+62 06 11.20	59 ± 3	122 ± 20	...	...
IRS 2a (W3A)	02 25 43.49	+62 06 10.76	73 ± 11	...	...	...
IRS 2b (W3A)	02 25 41.79	+62 06 24.07	82 ± 11	...	...	...
IRS 2c (W3A)	02 25 47.11	+62 06 13.02	69 ± 7	142 ± 19	...	...
IRS N2 (W3H)	02 25 32.59	+62 06 59.45	71 ± 5	93 ± 8	161 ± 21	743 ± 98
IRS N3 (W3J)	02 25 27.41	+62 03 42.97	47 ± 2	52 ± 4	89 ± 11	232 ± 29
IRS N4 (W3K)	02 25 44.86	+62 03 41.30	99 ± 6	80 ± 4	114 ± 21	...

Note.—Units of right ascension are hours, minutes, and seconds, and units of declination are degrees, arcminutes, and arcseconds.
[a] Naming conventions adopted from Wynn-Williams (1971), Wynn-Williams et al. (1972) and Harris & Wynn-Williams (1976).

0.15 mag corresponds to $A_V \sim 8.3$ mag. To redden a source with an intrinsic color of zero, characteristic of the background population, to the $[3.6] - [4.5] = 0.45$ mag bin requires $A_V \sim 25$ mag. Ojha et al. (2004) estimate an average extinction of $A_V \sim 15$ mag through the cluster around IRS 5. Maps by Kramer et al. (2004) show that the ^{13}CO line intensity is down by a factor of 10 or more in the Central Cluster region versus the region around IRS 5. Assuming a roughly linear relationship between ^{13}CO column depth and A_V, it is clear that the visual extinction in the Central Cluster cannot be as high as 25 mag and is therefore not responsible for the red excess.

We conclude that the red excess is due primarily to a population of sources with intrinsic infrared excess, such as YSOs. Previous near-infrared studies of the W3 Main region (Ojha et al. 2004; Megeath et al. 1996) have found a population of Class I and Class II YSOs, so it would not be surprising to find a similar population in the W3 region at large. Hartmann et al. (2005) show that typical colors of Class II YSOs lie in the range $0.2 \lesssim [3.6] - [4.5] \lesssim 0.7$, precisely the range in which the observed excess lies.

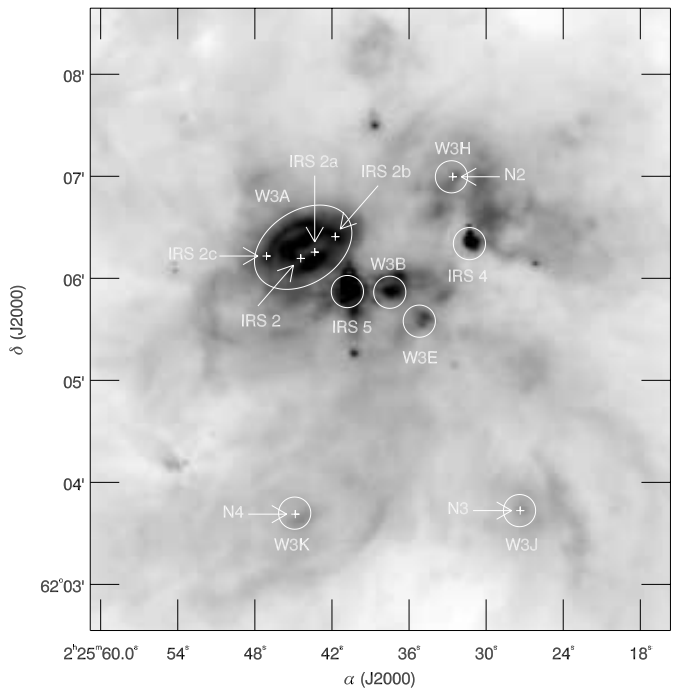

Fig. 4.—Image of the W3 Main area at 8.0 μm. The log of the flux is displayed. The circles mark well known luminous infrared sources and several compact and ultracompact H II regions. The crosses mark the locations of the embedded sources in Table 2.

The bottom row of Figure 6 shows star counts per square arcminute versus $[5.8] - [8.0]$ color. An excess of red sources is clearly visible. This red excess cannot be due to reddening. The 9.7 μm silicate feature contaminates the 8.0 μm bandpass so that extinction causes essentially no reddening in the $[5.8] - [8.0]$ color (Indebetouw et al. 2005). Any excess of red sources must therefore be due to a population of sources with an intrinsic

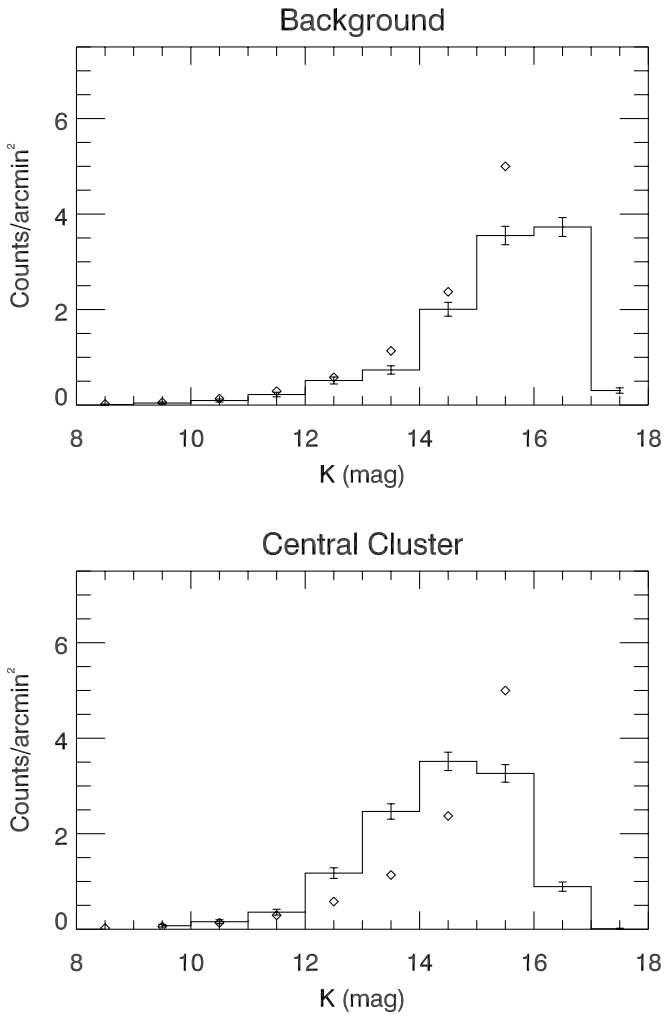

Fig. 5.—*K*-band luminosity function for the background (*top plot*) and the Central Cluster (*bottom plot*). The diamonds represent expected number of Galactic field stars in the direction of W3 (Garwood & Jones 1987). The completeness drops off sharply in the background after $K \sim 15$, and there is an overdensity of stars in the Central Cluster below $K \sim 15$.

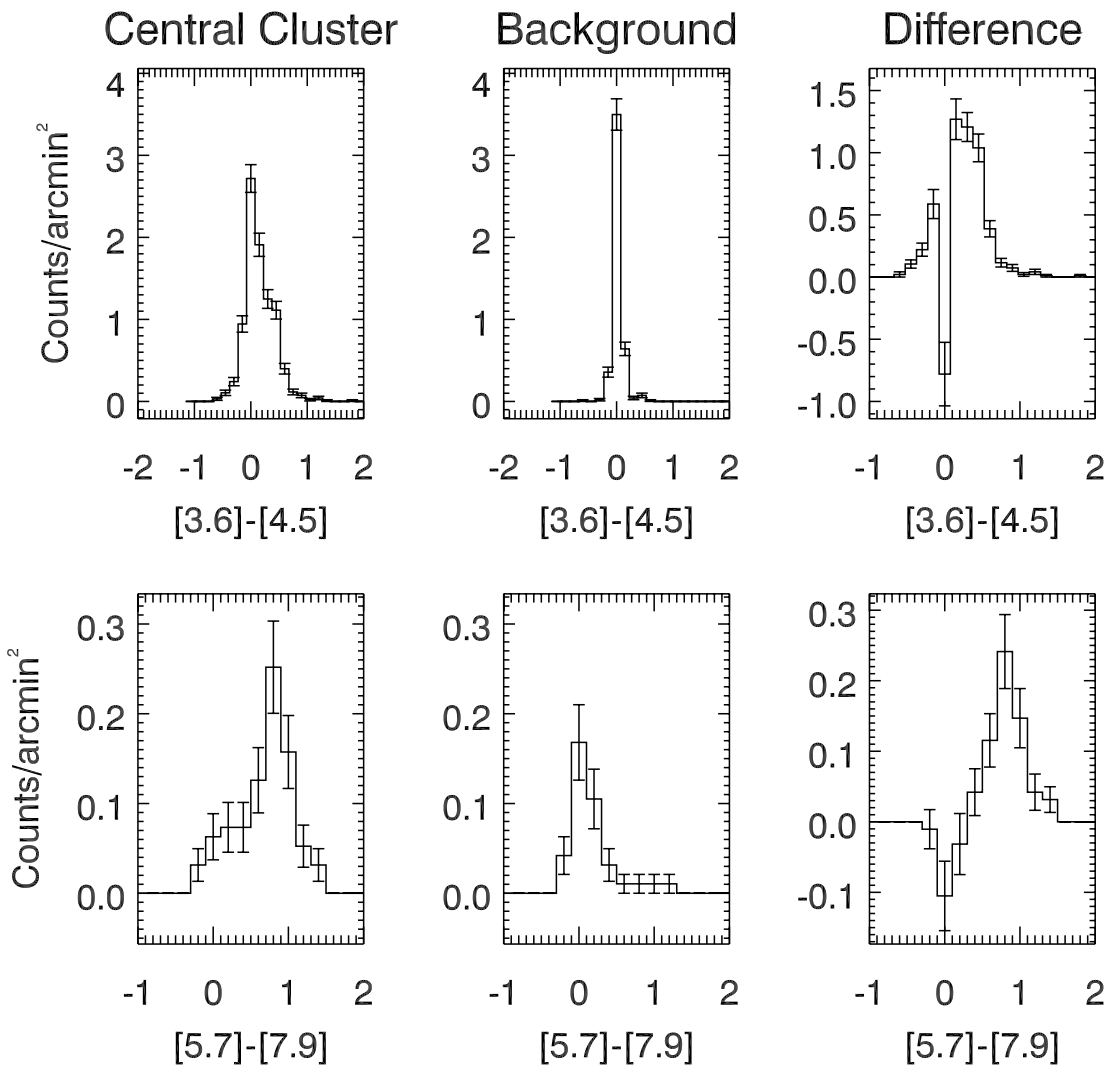

FIG. 6.—Star counts vs. color. The top row is [3.6]–[4.5] and the bottom row is [5.8]–[8.0]. The bin size is 0.15 mag in the top row, on the order of the error in the color. The bin size in the second row is 0.2 mag due to lower source count at 5.8 and 8.0 μm. The left column is counts in the Central Cluster, middle column is counts in the background, and right column is the difference. All counts are normalized by sky area. The difference curve shows an excess of red sources that we attribute to a population of stars with infrared excess.

infrared excess. The difference profile peaks at a color of 0.8, which is consistent with the colors of Class II and some Class I YSOs (Allen et al. 2004; Hartmann et al. 2005).

3.2. *Color-Color Diagrams*

YSOs occupy a distinct region of the IRAC color plane making the color-color diagram a powerful tool for YSO classification. In anticipation of the launch of the *Spitzer Space Telescope*, Whitney et al. (2003) and Allen et al. (2004) presented independent model predictions of the expected IRAC colors of various classes of YSO sources. Hartmann et al. (2005) later presented IRAC observations of independently classified Taurus pre-main-sequence objects verifying the Whitney and Allen model colors. Using the color-color diagram, we find a large group of new Class II YSO candidates in our images and show that a large fraction of them lie in the Central Cluster. The color-color diagram using both IRAC and MIPS 24 μm data is also a valuable diagnostic for YSO classification and we use it to strengthen the results obtained with or analysis of the IRAC color-color diagram.

The total number of point source detections in our sample drops sharply with increasing wavelength. Of the approximately 7200 detections at 3.6 and 4.5 μm, only 295 were also detected at 5.8 and 8.0 μm and only 38 were also detected at 24.0 μm. Figure 7 presents the $[5.8] - [8.0]$ versus $[3.6] - [4.5]$ color-color diagram containing the 295 sources that correlate between all four IRAC bands. The large circle centered at $[5.8] - [8.0] = 0.8$, and $[3.6] - [4.5] = 0.5$ represents the locus of Class II YSOs (Hartmann et al. 2005; Allen et al. 2004; Whitney et al. 2003). The solid box centered at $[5.8] - [8.0] = 0.0$ and $[3.6] - [4.5] = 0.0$ encloses the locus of "normal" stellar photospheres with little or no infrared excess. Hartmann et al. (2005) refers to sources in this locus as IRAC Class III, but in the case of W3 we expect this set to include many unreddened foreground and background stars as well as some Class III sources. We therefore choose to label this locus field star/Class III. Sources whose $[3.6] - [4.5]$ color lie redward of the Class II locus ($[3.6] - [4.5] \geq 0.9$) but whose $[5.8] - [8.0]$ color is consistent with or redder than a Class II source ($[5.8] - [8.0] \geq 0.4$) are interpreted as either reddened Class II sources or potential Class I sources, although the Class I/Class II division is not well defined, as we will discuss shortly. The reddening vector in Figure 7 is taken from Indebetouw et al. (2005) assuming $A_V/A_K = 7.5$. The error bars represent the mean photometric error derived from our photometry. Table 3 contains the photometry of all 295 sources discussed in this section.

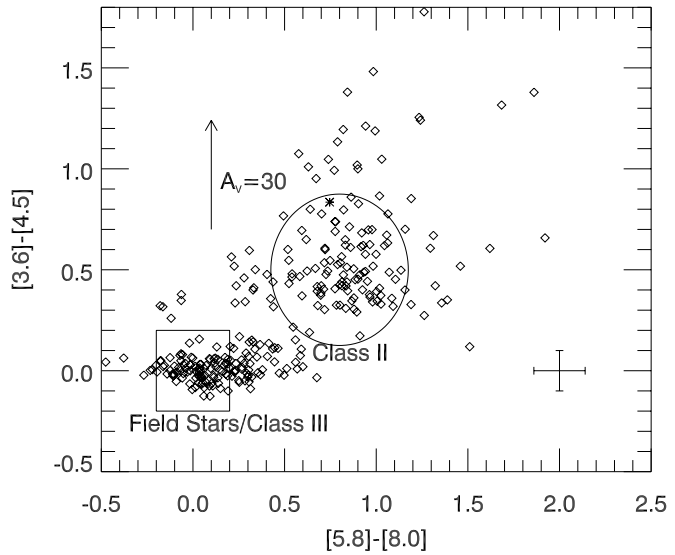

FIG. 7.—[3.6]–[4.5] vs. [5.8]–[8.0] color-color diagram of the 295 sources that correlate between all four IRAC bands. The reddening vector is taken from Indebetouw et al. (2005) assuming $A_V/A_K = 7.5$. Error bars represent the average photometric error. The asterisk is the source of the outflow discussed in § 3.3.

There are several potential sources of confusion in our classification. It is possible that some sources identified as Class II are actually reddened field star/Class III sources that were scattered into the Class II locus. It is also possible that some genuine Class II sources have been either scattered or reddened out of the Class II locus. It was also noted by Whitney et al. (2003) that the SEDs of highly inclined Class II sources closely resemble the SEDs, and therefore the colors, of Class I sources. In addition, Class I sources evolve into Class II sources (Adams et al. 1987; Whitney et al. 2003; Allen et al. 2004). Both of these facts make the boundary between Class I and Class II somewhat indistinct. Also, the distribution of sources clustered around the field star/Class III locus is elongated along the [5.8] − [8.0] axis. There is no spatial correlation between sources that lie within the area defined as field star/Class III and those that lie redward. The elongation could be due to increased photometric scatter in the long wavelength bands although the elongation is more redward than blueward. It most likely that the photometry is contaminated by bright nebulous emission in the 8.0 μm band.

The spatial distribution versus classification of the objects in Figure 7 reveals information about the stellar population of W3. In particular, the Central Cluster contains a large population of Class II sources and a deficit of Field Star/Class IIIs. Table 4 details the distribution both spatially and according to classification of the sources under consideration. There are several key features to note. Of all 295 sources, 26% are located in the Central Cluster and 12% are located in the background regions. In contrast, 51% of the sources identified as Class II are located in the Central Cluster and less than 1% are found in the background regions. Of the sources classified as field star/Class IIIs, 13% lie in the Central Cluster and 27% are located in the background regions. Although other authors (Ojha et al. 2004; Megeath et al. 1996) find a high density of YSO sources in the W3 Main region, only four of our sources are found in W3 Main, and only one is Class II. The lack of source detection is most likely due to high background levels in the 5.8 and 8.0 μm bands. We also detect eight Class II sources out of 19 detections in the W3(OH) region.

Adding the 24.0 μm data reduces the number of correlated sources from 295 to 38. However, an analysis of the color-color diagram including this data strengthens our results. In Figure 8 we present the [3.6] − [5.8] versus [8.0] − [24.0] color-color diagram containing the 38 sources that correlate in the IRAC bands and 24 μm. We refer to this diagram as IRAC+MIPS. Several regions for YSO classification have been mapped on this color plane by Muzerolle et al. (2004) and Reach et al. (2004). For this work, we have adopted the convention of Muzerolle et al. (2004). The symbols in Figure 8 represent the classification derived from Figure 7 color plane. With a few exceptions, the classifications are in very good agreement. Of the 21 sources identified as Class II, 19 lie within the IRAC+MIPS Class II locus. Of the seven sources identified as Class I, five lie within the IRAC+MIPS Class 0/I locus. No sources are detected in the field star/Class III locus given that these sources have little or no infrared excess and are below the 24.0 μm detection limit. Spatially, only 6 of the 39 sources lie within the Central Cluster. In fact, most of the sources lie in areas with relatively low background emission. But, 5 of these 6 sources in the Central Cluster are Class II. Overall, the IRAC+MIPS data support our analysis of the IRAC color plane.

TABLE 3
IRAC MAGNITUDES OF SOURCES DETECTED IN ALL FOUR BANDS

IRAC ID	2MASS ID	R.A. (J2000.0) (deg)	Decl. (J2000.0) (deg)	[3.6] (mag)	[4.5] (mag)	[5.8] (mag)	[8.0] (mag)	[24.0] (mag)
1.....	02243904+6203288	36.162575	62.058022	11.45 ± 0.09	10.84 ± 0.07	10.55 ± 0.08	9.69 ± 0.06	6.39 ± 0.13
2.....	02244314+6204011	36.179821	62.066978	12.77 ± 0.08	12.66 ± 0.11	12.54 ± 0.07	12.32 ± 0.09	...
3.....	02244570+6203512	36.190475	62.064205	12.08 ± 0.10	12.10 ± 0.08	11.93 ± 0.08	11.56 ± 0.11	...
4.....	02245191+6209367	36.216476	62.160172	10.12 ± 0.10	9.70 ± 0.08	9.45 ± 0.07	9.22 ± 0.05	7.53 ± 0.15
5.....	02245383+6210592	36.224472	62.183067	12.43 ± 0.09	12.36 ± 0.07	12.24 ± 0.09	11.89 ± 0.10	...
6.....	02244719+6201183	36.196861	62.021763	10.27 ± 0.07	10.21 ± 0.08	10.06 ± 0.08	9.79 ± 0.12	...
7.....	02244572+6158223	36.190521	61.972851	12.22 ± 0.08	12.27 ± 0.11	12.30 ± 0.08	12.02 ± 0.10	...
8.....	...	36.220528	62.078747	12.41 ± 0.08	11.20 ± 0.07	10.31 ± 0.06	9.37 ± 0.09	5.61 ± 0.13
9.....	02245870+6208263	36.244713	62.140594	13.22 ± 0.09	12.60 ± 0.09	11.91 ± 0.10	10.86 ± 0.10	...
10.....	02245578+6204264	36.232700	62.074162	13.12 ± 0.08	11.86 ± 0.09	10.93 ± 0.08	9.70 ± 0.14	5.98 ± 0.22
⋮	⋮	⋮	⋮	⋮	⋮	⋮	⋮	⋮
293.....	...	36.494740	62.141552	15.18 ± 0.21	11.86 ± 0.10	10.07 ± 0.08	8.99 ± 0.12	...
294.....	...	36.665749	61.956848	11.19 ± 0.12	10.70 ± 0.12	10.25 ± 0.14	9.52 ± 0.12	...
295.....	02260117+6202245	36.505135	62.040066	10.95 ± 0.12	10.12 ± 0.10	10.46 ± 0.14	9.72 ± 0.19	3.64 ± 0.13

NOTE.—Table 3 is published in its entirety in the electronic edition of the *Astrophysical Journal*. A portion is shown here for guidance regarding its form and content.

TABLE 4
Distribution of Sources Detectable in All Four IRAC Bands

Region	All	Class I	Class II	Field star/Class III
All	295	21	94	88
Central Cluster	79	0	48	11
Background	39	1	4	24
W3 Main	4	1	1	0
W3(OH)	19	3	8	0

Although we detect only 295 sources at 5.8 and 8.0 μm out of the more than 7000 sources detected at 3.6 and 4.5 μm and only 38 sources when we add 24 μm, the color-color diagrams coupled with the information presented in § 3.1 and CO maps by Kramer et al. (2004) presents a compelling picture of the stellar composition of the region. The CO maps show reduced column densities of molecular gas in the Central Cluster with respect to the W3 Main and W3 OH regions. In both the CO maps and the IRAC images, there are filaments connecting W3 main and W3 OH suggesting that all three regions are part of the same complex. It is in the Central Cluster that we identify the greatest density of Class II sources. On the outskirts of the Central Cluster lies a source with a visible outflow, discussed in § 3.3. The outflow source shows colors of an early Class II/late Class I system. In addition, several Class I sources lie very near the edge of the Central Cluster and none lie within it. We suggest that the Central Cluster resides in a cavity cleared by an earlier episode of star formation and that we see triggered star formation at the edges of this cavity, consistent with the hypothesis by Oey et al. (2005).

3.3. *A New Outflow*

Figure 9 shows the region around a potential Class I YSO with an associated outflow. The top panel is a 4.5 μm image and the bottom panel is the ratio of the 4.5 μm image to the 3.6 μm image. The morphology of the source and associated outflow is complex and there are several interesting features highlighted in Figure 9. Primarily, there is an outflow extending from southeast to northwest that is extremely bright at 4.5 μm. Near the southeast focus of the ellipse in Figure 9 we can see the source of the outflow along with a fan of nebulosity extending to the northwest. Two loops of emission as well as several knots can be clearly seen along the outflow axis. The spatial extent of the outflow is approximately 0.62 pc. These features, especially the northwest loop, are strikingly similar in appearance and of comparable spatial extent, approximately 0.5 pc, to IRAC observations of the HH 46/47 system by Noriega-Crespo et al. (2004). Table 5 lists the positions of the important features.

In the 4.5 to 3.6 μm ratio image we note that the source and its reflection nebula have essentially vanished but the loops and the knots have been enhanced due to the strength of the emission at 4.5 μm. At 5.8 and 8.0 μm as well as *J*, *H*, and *K* images from the 2MASS database, the loops and knots are not evident. We are most likely seeing emission from a shock at the outflow boundary. Noriega-Crespo et al. (2004) report that the shocked emission in the case of HH 46/47 is most likely due to H_2 rotational transitions. We could also be detecting emission from Brα at

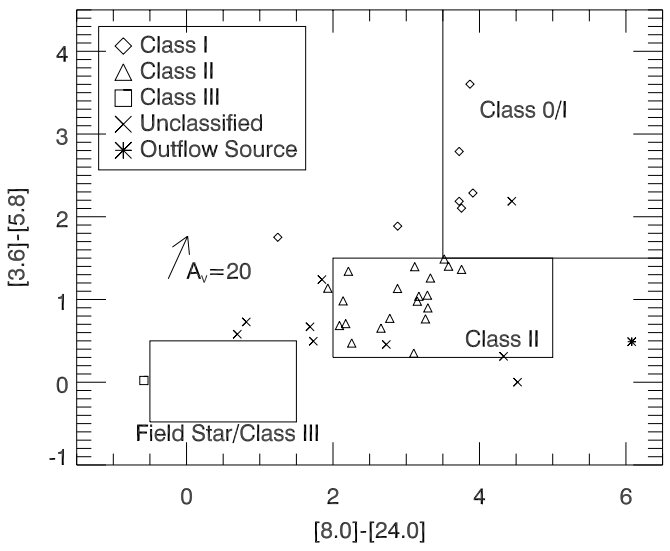

Fig. 8.—[3.6]–[5.8] vs. [8.0]–[24.0] color-color diagram of the 38 MIPS sources that correlate with sources in Fig. 7. The reddening vector is derived from Mathis (1990). The symbols represent the YSO classification obtained from Fig. 7. There is very good agreement between the two classifications. The asterisk is the source of the outflow discussed in § 3.3.

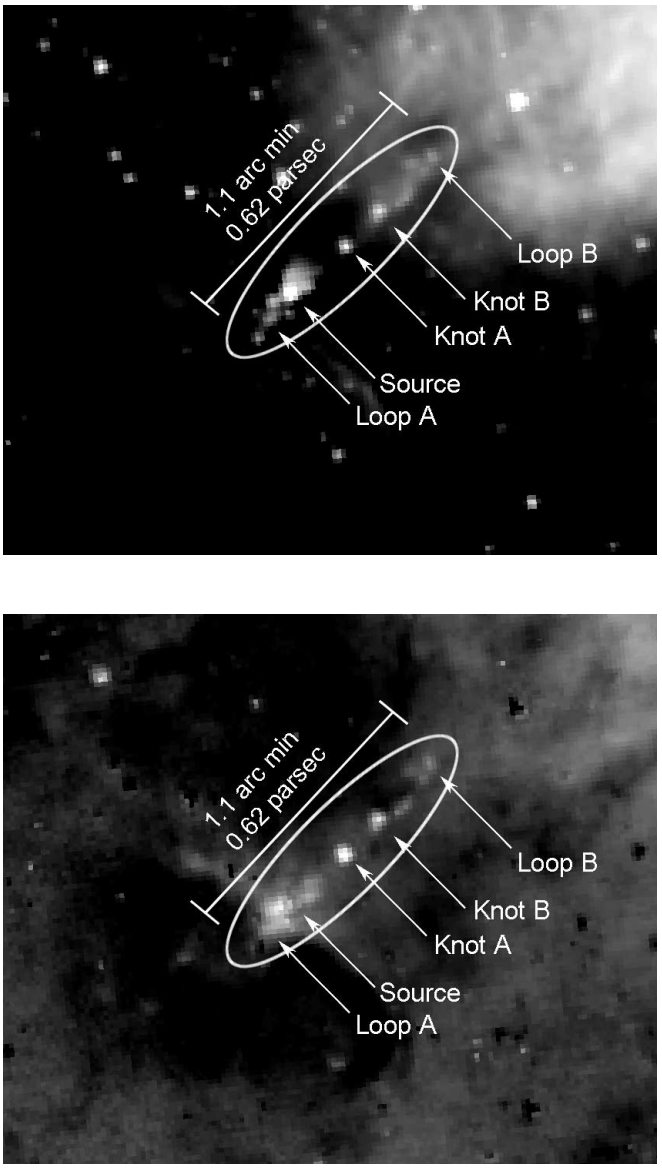

Fig. 9.—Close-up images of a new outflow and its candidate source discovered in the IRAC images. The top panel is a 4.5 μm image and the bottom panel is the ratio of 4.5 to 3.6 μm. The outflow is much brighter at 4.5 μm than at the other bands. The features labeled as knots and loops may be shock fronts due to the outflow (cf. Noriega-Crespo et al. 2004).

TABLE 5
Positions of Outflow Features

Feature	R.A. (J2000.0)	Decl. (J2000.0)
Source.....	02 26 01.23	+62 02 24.2
Knot *A*.....	02 25 59.37	+62 02 36.5
Knot *B*.....	02 25 57.87	+62 02 46.6
Loop *A*	02 26 02.05	+62 02 17.2
Loop *B*	02 25 55.90	+62 03 00.4

Note.—Units of right ascension are hours, minutes, and seconds, and units of declination are degrees, arcminutes, and arcseconds.

4.05 μm, which appears at the edge of 4.5 μm band or from the CO band from 4.6 to 4.8 μm. Spectra are needed to fully characterize the outflow.

In Figure 10 we present the SED of the outflow source. The source was also detected by 2MASS and those data points are represented by diamonds. The SED rises steeply through *J*, *H*, *K*, and 3.6 μm peaks at 4.5 μm declines sharply at longer to 8.0 μm and shows a significant excess at 24 μm. We calculate a [3.6] − [4.5] color of 0.83 ± 0.11 mag and a [5.8] − [8.0] color of 0.74 ± 0.18 mag, which places it just outside of the Class II locus on the color-color plane (Fig. 7), suggesting that it is likely a late Class I source. The dip at 8.0 μm could be due to silicate absorption suggesting that this is an embedded source.

4. CONCLUSIONS

We have presented new images of the W3 region, including W3(OH), and W3 Main. In the W3(OH) region, the ultracompact H II region and the hot molecular core were saturated. The most luminous sources in W3 Main, IRS 4, and IRS 5 were also saturated in our images.

The photometry of over 7000 point sources in the W3 region enables us to present a statistical analysis of the overall stellar population. Examining star counts versus [3.6]–[4.5] color, we find that the Central Cluster region has an enhanced population of red sources versus the background and a lack of "normal" sources, those with a color of zero. It is unlikely that the red enhancement is caused by reddening due to extinction. Instead, we attribute this enhancement to a collection of sources with an intrinsic infrared excess. Furthermore, the colors of the red population are shown to be consistent with a collection of Class II YSOs. An examination of star counts versus [5.8]–[8.0] color yields similar results. An enhancement of red sources in the Central Cluster versus the background is shown. Reddening due to extinction is discounted and it is shown that the colors are consistent with a collection of Class I/II YSOs.

A [5.8]–[8.0] versus [3.6]–[4.5] color-color diagram of all sources in our data set that correlate between all four IRAC bands and a color-color diagram including MIPS 24 μm are presented. We note the presence of a large fraction of sources within the Class II locus. Spatially, a large fraction of sources in the Class II locus lie within the Central Cluster, while a very small fraction lie in the background regions.

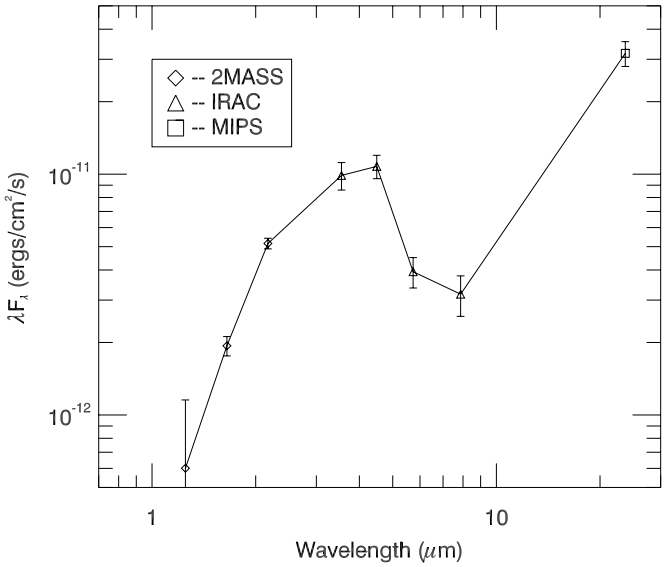

Fig. 10.— SED of the candidate exciting star associated with the outflow in Fig. 9.

We also present the detection of a previously unknown outflow along with its candidate source. The outflow resides at the edge of the Central Cluster and is much brighter at 4.5 μm than the other bands. A large loop and several knots of shocked gas are apparent. The source displays extensive reflection nebulosity and has colors consistent with a late Class I YSO.

We suggest that the Central Cluster resides in a cavity that was cleared by a previous episode of star formation and that the areas of active star formation, W3 Main and W3(OH), were potentially triggered by this earlier event, findings that are consistent with Oey et al. (2005). The low CO column density in the Central Cluster, the large number of YSO sources, the lack of luminous embedded sources, the location on the outskirts of the cavity of the luminous embedded young clusters such as those in W3 Main and W3(OH), and the location on several protostars (Class I sources) around the edges of the cavity support our conclusion.

G. R., C. E. W., E. P., and R. D. G. are supported in part by NASA through *Spitzer* contracts 1256406 and 1215746 issued by JPL/Caltech to the University of Minnesota, and by National Science Foundation grant AST02-05814. This publication makes use of data products from the Two Micron All Sky Survey, which is a joint project of the University of Massachusetts and the Infrared Processing and Analysis Center/California Institute of Technology, funded by the National Aeronautics and Space Administration and the National Science Foundation. Support for S. T. M was provided by NASA through contract 1256790 issued by JPL/Caltech

REFERENCES

Adams, F. C., Lada, C. J., & Shu, F. H. 1987, ApJ, 312, 788
Allen, L. E., et al. 2004, ApJS, 154, 363
Dreher, J. W., & Welch, W. J. 1981, ApJ, 245, 857
Fazio, G. G., et al. 2004, ApJS, 154, 10
Garwood, R., & Jones, T. J. 1987, PASP, 99, 453
Harris, S., & Wynn-Williams, C. G. 1976, MNRAS, 174, 649
Hartmann, L., Megeath, S. T., Allen, L., Luhman, K., Calvet, N., D'Alessio, P., Franco-Hernandez, R., & Fazio, G. 2005, ApJ, 629, 881
Indebetouw, R., et al. 2005, ApJ, 619, 931
Kramer, C., Jakob, H., Mookerjea, B., Schneider, N., Brüll, M., & Stutzki, J. 2004, A&A, 424, 887
Makovoz, D., & Khan, I. 2005, in ASP Conf. Ser. 347, ed. P. Shopbell, M. Britton, & R. Ebert, (San Francisco: ASP), 81
Mathis, J. S. 1990, ARA&A, 28, 37
Megeath, S. T., Herter, T., Beichman, C., Gautier, N., Hester, J. J., Rayner, J., & Shupe, D. 1996, A&A, 307, 775

Muzerolle, J., et al. 2004, ApJS, 154, 379
Noriega-Crespo, A., et al. 2004, ApJS, 154, 352
Oey, M. S., Watson, A. M., Kern, K., & Walth, G. L. 2005, AJ, 129, 393
Ojha, D. K., et al. 2004, ApJ, 608, 797
Reach, W. T., et al. 2004, ApJS, 154, 385
Rieke, G. H., et al. 2004, ApJS, 154, 25
Stetson, P. B. 1987, PASP, 99, 191
Turner, J. L., & Welch, W. J. 1984, ApJ, 287, L81
Whitney, B. A., Wood, K., Bjorkman, J. E., & Cohen, M. 2003, ApJ, 598, 1079
Wynn-Williams, C. G. 1971, MNRAS, 151, 397
Wynn-Williams, C. G., Becklin, E. E., & Neugebauer, G. 1972, MNRAS, 160, 1
Xu, Y., Reid, M. J., Zheng, X. W., & Menten, K. M. 2006, Science, 311, 54